JOURNAL OF MATERIALS SCIENCE 14 (1979) 1398–1406

Tempering of a beta quenched Zr–1.9 wt % Cr alloy

Part 2 *$ZrCr_2$ precipitation*

P. MUKHOPADHYAY, V. RAMAN, S. BANERJEE, R. KRISHNAN
Metallurgy Division, Bhabha Atomic Research Centre, Bombay-400 085, India

The precipitation of $ZrCr_2$, which is a Laves phase with the C15 structure, in a supersaturated, martensitic matrix has been studied in a Zr–1.9 wt % Cr alloy using transmission electron microscopy. The nucleation, morphology and distribution of the precipitates has been examined at different tempering temperatures. The crystallographic orientation relationship between the α-Zr(Cr) and the $ZrCr_2$ phases has been established and the precipitate habit plane determined.

1. Introduction

The $ZrCr_2$ phase is the only intermetallic phase that has been reported to form in the binary zirconium–chromium system [1]. Structure-wise it is a Laves phase and exhibits the general geometrical characteristics associated with these phases. It evolves through the eutectoidal decomposition of the β-Zr(Cr) phase and thus can be made to form by isothermal transformation at sub-eutectoid temperatures. In dilute alloys, where it is possible to obtain a supersaturated martensite by rapid beta quenching, this phase can also be precipitated by tempering the martensite at temperatures in the α-Zr(Cr) + $ZrCr_2$ field. This mode of the evolution of the $ZrCr_2$ phase has been studied earlier by Keys *et al.* [2] who have used transmission electron microscopy to examine the shape and the distribution of the precipitates. However, no work seems to have been done so far on the crystallography of this precipitation reaction. In the work described in this chapter the mode of precipitation of $ZrCr_2$ was studied in a Zr–1.9 wt % Cr alloy. In particular, the crystallography of the process was examined and the matrix–precipitate orientation relationship established. Precipitation was brought about by tempering the beta quenched alloy at sub-eutectoid temperatures.

Two structural variants of $ZrCr_2$ have been reported. Both are topologically close-packed Laves phase structures: C14 (hexagonal, $MgZn_2$ type) with $a = 5.079$ Å, $c = 8.279$ Å and C15 (cubic, $MgCu_2$ type) with $a = 7.21$ Å [3]. However, there has been a disagreement among various workers as to the temperature ranges associated with these two structural variants. According to Rostoker [3] and Elliott [4], $ZrCr_2$ has the C14 structure below about 1000° C and the C15 structure at higher temperatures. On the other hand, Alisova *et al.* [5] and Jordan and Duwez [6] have suggested that the low temperature form has the C15 structure and that the transformation temperature is close to the melting point of $ZrCr_2$. Later work by Shen and Paasche [7] and by Rumball and Elder [8] has demonstrated that the cubic form is indeed stable at low temperatures. In view of this, it was assumed in this work that the $ZrCr_2$ precipitates forming in the α-Zr(Cr) matrix had the C15 structure with $a = 7.21$ Å.

2. Unit cell of $ZrCr_2$

The C15 unit cell of $ZrCr_2$ is shown in Fig. 1. Following the choice of origin adopted in [1], the atomic co-ordinates are:

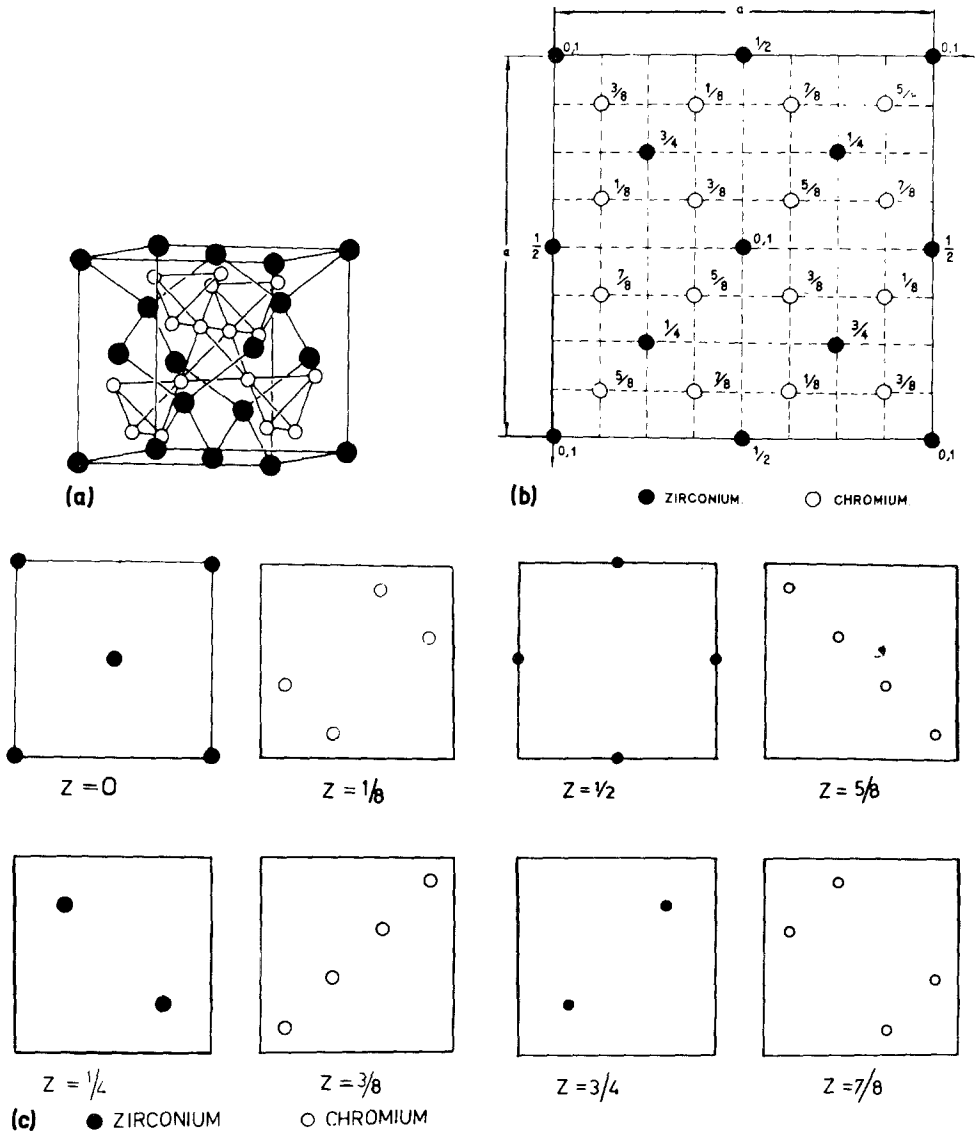

Figure 1 (a) The C15 unit cell of $ZrCr_2$. (b) The positions of the atoms in the unit cell, when viewed along the $[0\,0\,\bar{1}]$ direction. The numbers and fractions indicate the value of z, the vertical distance from the plane of the paper. (c) The atomic arrangement in the eight layers parallel to the (0 0 1) plane whose successive stacking builds up the $ZrCr_2$ unit cell.

zirconium: $000; 0\tfrac{1}{2}\tfrac{1}{2}; \tfrac{1}{2}0\tfrac{1}{2}; \tfrac{1}{2}\tfrac{1}{2}0;$

$\tfrac{1}{4}\tfrac{1}{4}\tfrac{1}{4}; \tfrac{1}{4}\tfrac{3}{4}\tfrac{3}{4}; \tfrac{3}{4}\tfrac{1}{4}\tfrac{3}{4}; \tfrac{3}{4}\tfrac{3}{4}\tfrac{1}{4}$

chromium: $\tfrac{5}{8}\tfrac{5}{8}\tfrac{5}{8}; \tfrac{5}{8}\tfrac{7}{8}\tfrac{7}{8}; \tfrac{7}{8}\tfrac{5}{8}\tfrac{7}{8}; \tfrac{7}{8}\tfrac{7}{8}\tfrac{5}{8};$

$\tfrac{5}{8}\tfrac{1}{8}\tfrac{1}{8}; \tfrac{5}{8}\tfrac{3}{8}\tfrac{3}{8}; \tfrac{7}{8}\tfrac{1}{8}\tfrac{3}{8}; \tfrac{7}{8}\tfrac{3}{8}\tfrac{1}{8};$

$\tfrac{1}{8}\tfrac{5}{8}\tfrac{1}{8}; \tfrac{1}{8}\tfrac{7}{8}\tfrac{3}{8}; \tfrac{3}{8}\tfrac{5}{8}\tfrac{3}{8}; \tfrac{3}{8}\tfrac{7}{8}\tfrac{1}{8};$

$\tfrac{1}{8}\tfrac{1}{8}\tfrac{5}{8}; \tfrac{1}{8}\tfrac{3}{8}\tfrac{7}{8}; \tfrac{3}{8}\tfrac{1}{8}\tfrac{7}{8}; \tfrac{3}{8}\tfrac{3}{8}\tfrac{5}{8}.$

The chromium atoms form a tetrahedral network, the adjacent tetrahedra being joined at the vertices. The zirconium atoms occupy the holes provided by these tetrahedra and are themselves arranged in a manner identical to that obtained in the diamond cubic structure. The entire structure can be built up by the consecutive stacking of eight planes parallel to the (0 0 1) plane as shown in Fig. 1c. Ideally, the closest distance between zirconium atoms is $\sqrt{3}a/4$ and that between chromium atoms is $a/2\sqrt{2}$ where a is the unit cell edge. This is illustrated in Fig. 2 which shows the atomic arrangement on the (1 1 0) plane. The closest distance between dissimilar atoms is $\sqrt{11}a/8$. Each zirconium atom is surrounded by four

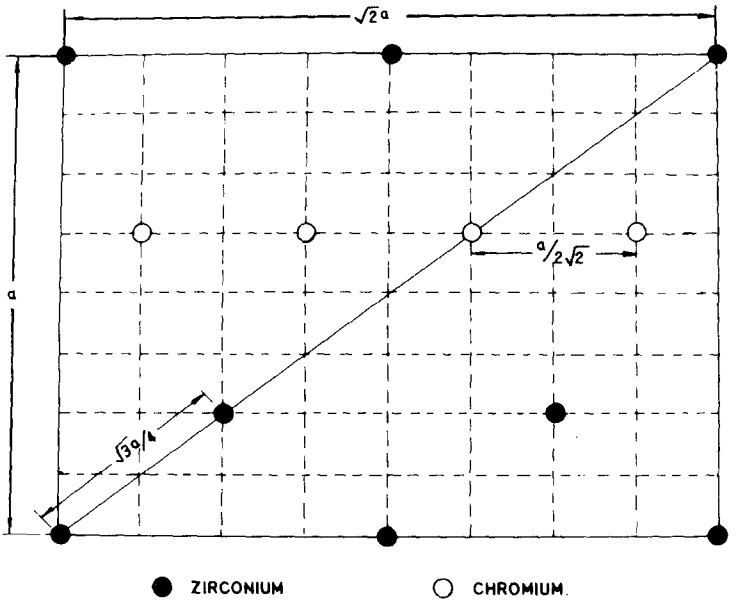

Figure 2 The atomic arrangement on the (1 1 0) plane of $ZrCr_2$.

zirconium atoms (at a distance $\sqrt{3}a/4$) and twelve chromium atoms (at a distance $\sqrt{11}a/8$). These sixteen atoms occupy the vertices of the CN16 co-ordination polyhedron. Each chromium atom, on the other hand, is surrounded by a CN12 co-ordination polyhedron whose vertices are occupied by six chromium atoms (at a distance $a/2\sqrt{2}$) and six zirconium atoms (at a distance $\sqrt{11}a/8$). The CN16 polyhedra around the zirconium atoms form close-packed layers parallel to the (1 1 1) plane and are so stacked that there is a rotation of 60° between any two successive layers [9]. The actual interatomic distances are slightly different from those mentioned here because the latter values are strictly valid for an ideal radius ratio of 1.225. For $ZrCr_2$, the radius ratio is 1.250, on the basis of the CN12 atomic radii computed by Teatum *et al.* [10].

TABLE I Algebraic expressions for F^*F for some common $ZrCr_2$ reflections, assuming perfect long-range order

Reflection $\{h\,k\,l\}$	Interplanar spacing (Å)	Algebraic expression for F^*F
1 1 1	4.163	$2(4f_{Zr} - 5.7f_{Cr})^2$
2 2 0	2.549	$64f_{Zr}^2$
3 1 1	2.174	$2(4f_{Zr} + 5.7f_{Cr})^2$
2 2 2	2.081	$256f_{Cr}^2$
4 0 0	1.803	$(8f_{Zr} - 16f_{Cr})^2$
3 3 1	1.654	$2(4f_{Zr} - 5.7f_{Cr})^2$
4 2 2	1.472	$64f_{Zr}^2$
3 3 3	1.388	$2(4f_{Zr} + 5.7f_{Cr})^2$
5 1 1	1.388	$2(4f_{Zr} + 5.7f_{Cr})^2$
4 4 0	1.275	$(8f_{Zr} + 16f_{Cr})^2$
5 3 1	1.219	$2(4f_{Zr} - 5.7f_{Cr})^2$
6 2 0	1.140	$64f_{Zr}^2$
5 3 3	1.100	$2(4f_{Zr} + 5.7f_{Cr})^2$
6 2 2	1.087	$256f_{Cr}^2$
4 4 4	1.041	$(8f_{Zr} - 16f_{Cr})^2$

3. Structure factor of $ZrCr_2$

The algebraic expressions for the structure factor were obtained, assuming perfect long-range order, for several common, low index reflections in terms of f_{Zr} and f_{Cr}, the atomic scattering amplitudes for zirconium and chromium, respectively. It was found that only those reflections $\{h\,k\,l\}$ were permitted for which h, k and l were all odd or all even. This was expected since the C15 unit cell of $ZrCr_2$ is face centred. The computed values of F^*F, where F is the structure factor and F^* its complex conjugate, for several non-vanishing reflections are given in Table I. The interplanar spacings of the planes associated with these reflections are also shown.

4. Observations and discussions

4.1. Nucleation, morphology and distribution of precipitates

The majority of the $ZrCr_2$ precipitation formed during beta quenching was found to be nucleated within the martensite plates (Fig. 3), very often on the dislocations within these. The presence of the precipitates in the beta quenched alloy suggested that since the solubility of chromium in alpha zirconium is negligible at low temperatures,

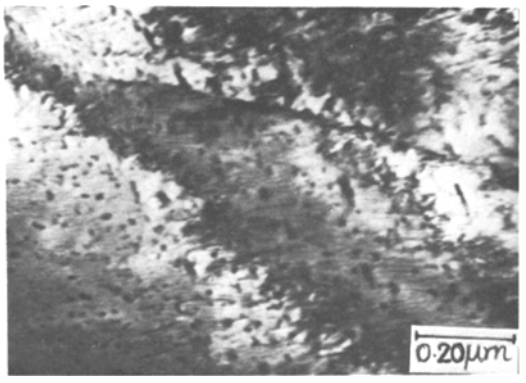

Figure 3 Precipitation of $ZrCr_2$ within the martensite plates in the beta quenched alloy.

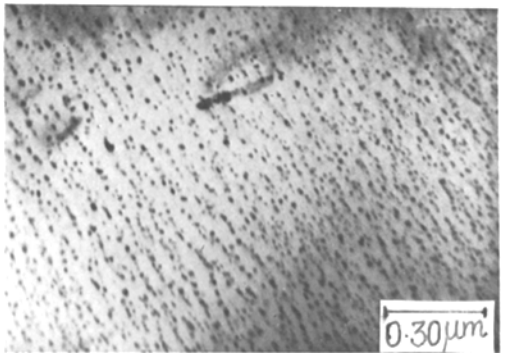

Figure 4 Alignment of precipitates along lines (giving the appearance of "discontinuous lamellae" of the precipitate phase) in the beta quenched alloy.

solute rejection occurred at such a rapid rate that it could not be suppressed even by the fast rate of cooling employed. In fact, in certain regions of one sample the structure resembled the product of a discontinuous precipitation reaction. The precipitate particles in regions appeared to be aligned along more or less parallel, wavy lines (Fig. 4). It was possible that these rows of precipitates trailed the advancing transformation front at which the beta phase rejected the alpha and $ZrCr_2$ phases simultaneously. In other words, direct eutectoid transformation [11] had set in in these regions. Such a situation would have been possible when the supercooling was sufficient for this process to occur in the hypereutectoid alloy studied. These observations were suggestive of the fact that in the beta quenched alloy the martensitic transformation and the direct eutectoid decomposition processes were competitive.

On tempering at 350° C, the precipitates at the martensite interfaces were seen to have grown much larger than those within the bulk. This is illustrated in Fig. 5 which shows large, heterogeneously nucleated, cuboidal precipitates along the martensite plate boundaries together with a fine, homogenously nucleated precipitate dispersion within the plates. Occasionally, the larger precipitates at the boundaries appeared to tend to join up to form "stringers" (Fig. 6a). The corresponding selected-area diffraction pattern showed a superposition of alpha and $ZrCr_2$ reflections (Fig. 6b). Unambiguous identification of the precipitate phase could be carried out on the basis of such diffraction patterns and of dark-field imaging. It was noticed that in some regions the precipitates within the laths had grown to assume elongated shapes, as shown in Fig. 7.

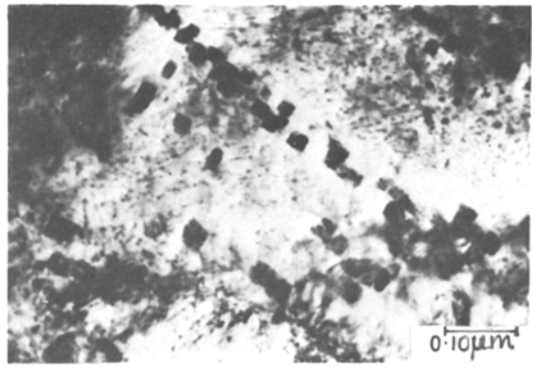

Figure 5 Distribution of large, heterogeneously nucleated, cuboidal precipitates and of fine, homogeneously nucleated precipitates in the alloy on ageing at 350° C for 16 h.

On raising the ageing temperature to 550° C, precipitation was found to be more extensive and the bimodal size distribution persisted (Fig. 8a). It was generally observed (at 550° C as well as at 350° C) that the precipitates which nucleated at boundaries or at dislocations were larger than those homogeneously nucleated in the matrix. This was presumably due to the fact that while the former grew by short circuit diffusion, the latter could grow only with the assistance of the much slower process of volume diffusion. The majority of the precipitation in samples tempered at 550° C were found to be cuboidal in shape – even those within the laths were found to develop a cuboidal morphology (Fig. 8b). This micrograph also shows another general feature of the microstructure in that many of these cuboidal precipitates were threaded by dislocations, giving an appearance of "stringers".

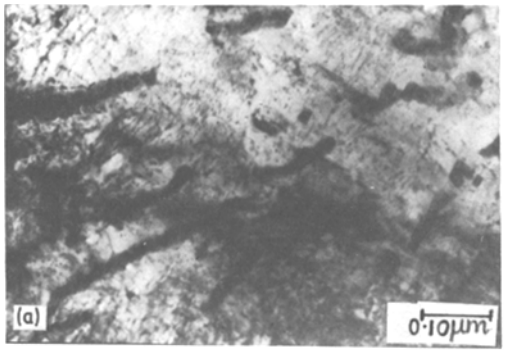

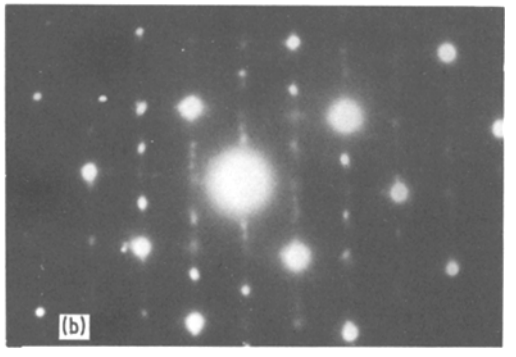

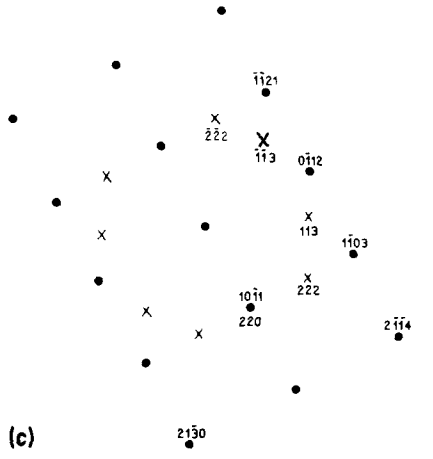

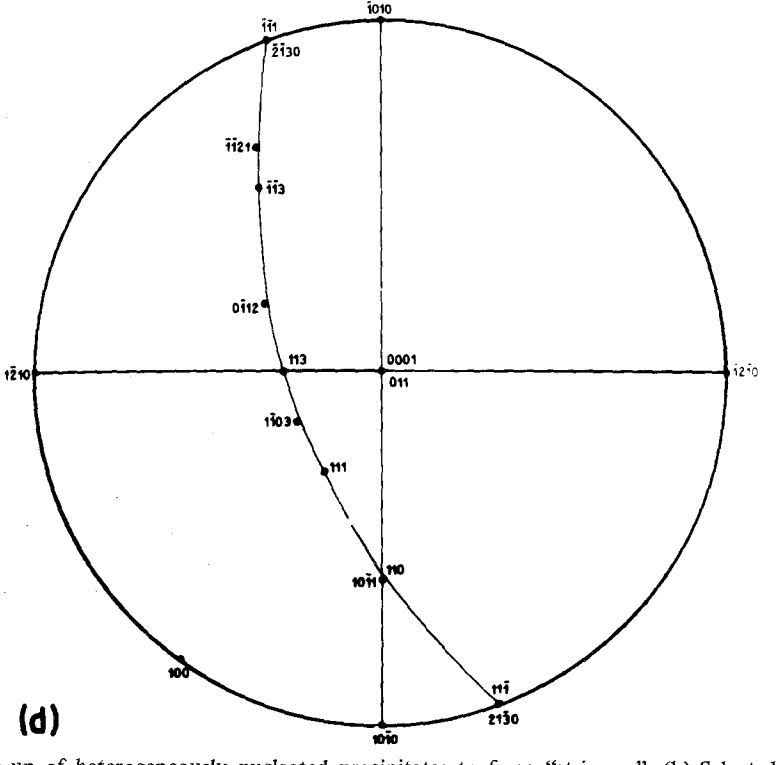

Figure 6 (a) Joining up of heterogeneously nucleated precipitates to form "stringers". (b) Selected-area diffraction pattern from the region shown in (a). The zone axis is of the $\langle 5\,\bar{1}\,\bar{4}\,3\rangle$ type in terms of alpha zirconium and of the $\langle 1\,\bar{\bar{1}}\,0\rangle$ type in terms of $ZrCr_2$. (c) Key to the diffraction pattern in (b). The additional spots in (b) not shown in (c) are due to other precipitate variants and due to double diffraction. (d) Stereogram corresponding to (b) showing that the following orientation relation between the α-Zr(Cr) and the $ZrCr_2$ phases could be arrived at: $(0\,0\,0\,1) \parallel (0\,1\,1)$ and $[2\,1\,\bar{3}\,0] \parallel [1\,1\,\bar{1}]$.

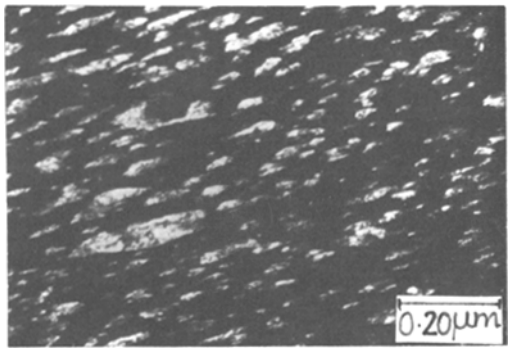

Figure 7 Elongated precipitates in a lath observed on ageing at 350° C, imaged with a $ZrCr_2$ reflection.

In samples tempered at 700° C, a significant extent of precipitate coarsening was found to have occurred both at the interfaces and within the grains (Fig. 9). This growth appeared to have taken place at the expense of the fine precipitates observed at the lower tempering temperatures. Dark-field imaging revealed that these coarsened precipitates were not cuboidal but were plate-shaped. It was observed that the dimensions along the flat side of the plates were not much larger than the plate thickness (Fig. 10). It was also observed that the flat face of many of these precipitates contained quite a number of ledges. This suggested that precipitate growth occurred by the ledge growth mechanism [12].

4.2. Crystallography of precipitation

It was possible to determine the orientation relation between the alpha and $ZrCr_2$ phases by means of selected-area diffraction. In order to obtain an unambiguous result, superimposed reciprocal lattice sections of matrix and precipitate crystals, corresponding to different zones, were analysed. Typical results are presented in Fig. 11. In Fig. 11a, the diffraction pattern shows that the (0 1 1) and $(4\,4\,\bar{4})$ spots of $ZrCr_2$ nearly coincide with the $(0\,0\,0\,2)_\alpha$ and the $(2\,1\,\bar{3}\,0)_\alpha$ spots, respectively. Using this information, a stereographic plot (superimposing the (0 1 1) projection of $ZrCr_2$ and the (0 0 0 1) projection of alpha zirconium) was obtained where the $(1\,1\,\bar{1})$ pole of $ZrCr_2$ was made to match with the $(2\,1\,\bar{3}\,0)_\alpha$ pole (Fig. 12). The orientation relationship between the two phases could be expressed in terms of

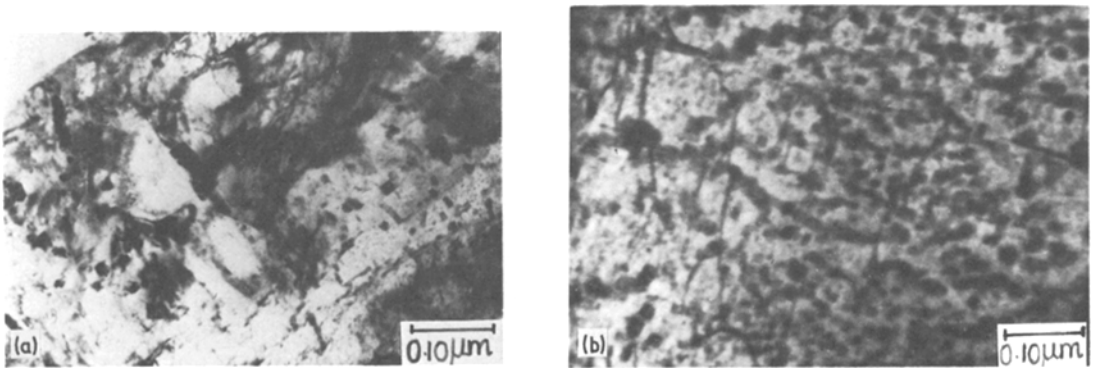

Figure 8 (a) Bimodal precipitate size distribution observed on tempering the alloy at 550° C for 4 h. (b) Zr–1.9 wt % Cr, beta quenched and aged at 550° C for 4 h. Cuboidal morphology of $ZrCr_2$ precipitates formed within a lath.

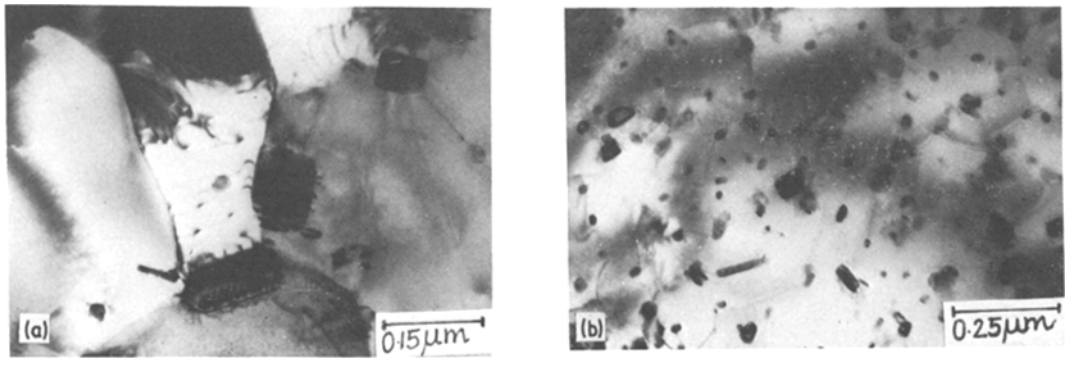

Figure 9 Coarse $ZrCr_2$ precipitates at (a) interfaces as well as (b) within grains in a sample aged at 700° C for 4 h.

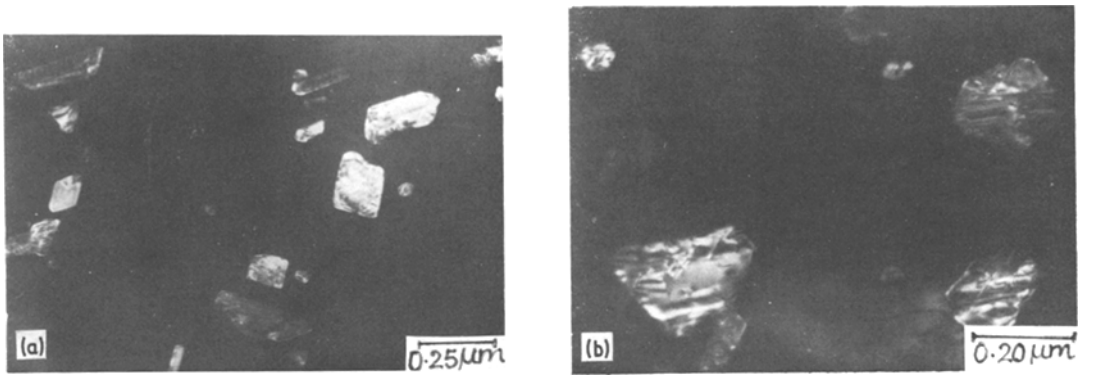

Figure 10 (a) and (b) Dark-field images of coarse, plate-shaped $ZrCr_2$ precipitates demonstrating that the dimensions along the flat face of the plates were not much larger than the plate thickness and that the flat faces often contained ledges.

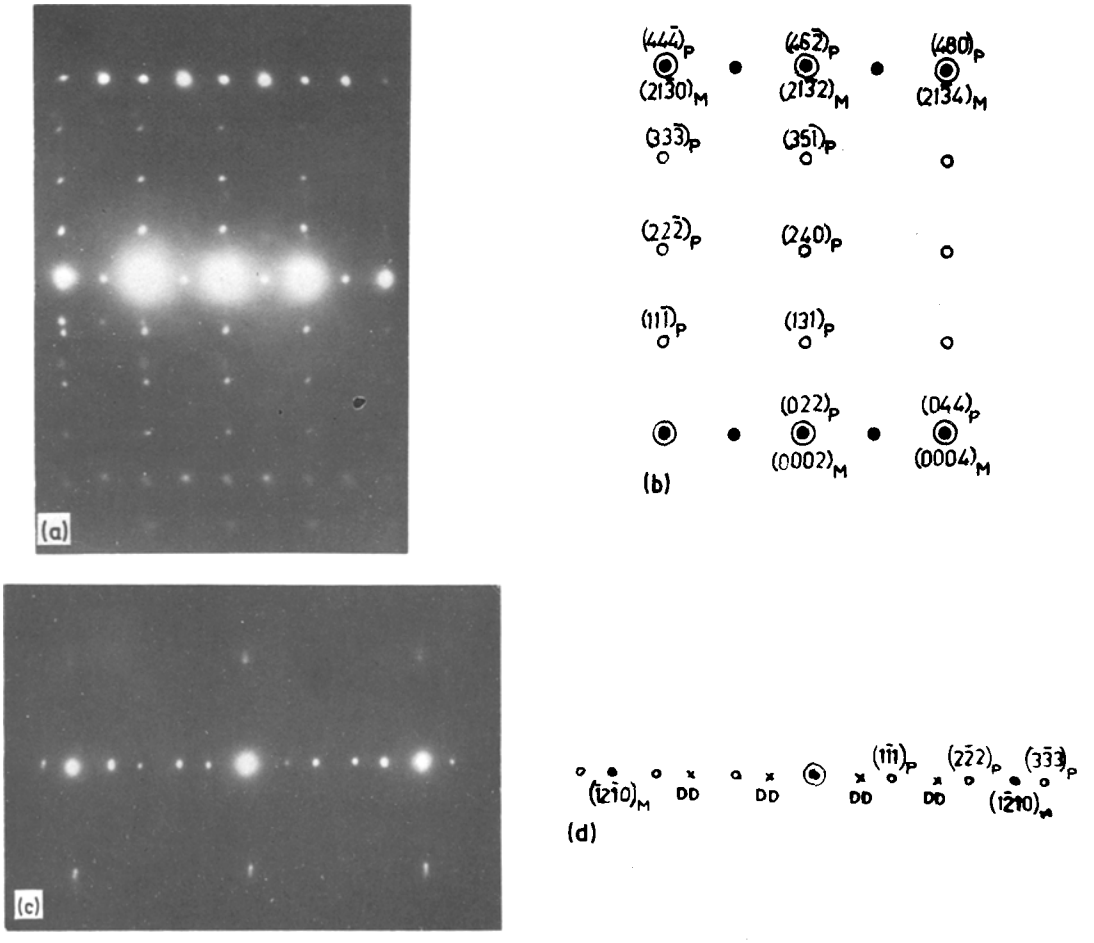

Figure 11 (a) Selected-area diffraction pattern illustrating the orientation relationship between the α-Zr(Cr) and the $ZrCr_2$ phases. The zone axis is of the ⟨4 $\bar{5}$ 1 0⟩ type in terms of α-Zr(Cr) and of the ⟨0 $\bar{1}$ 1⟩ type in terms of $ZrCr_2$. (b) Key to the diffraction pattern in (a). (c) Selected-area diffraction pattern showing α-Zr(Cr) and $ZrCr_2$ reflections. This pattern was consistent with the orientation relation derived from (a) and illustrated in Fig. 12. The zone axis is of the ⟨1 0 $\bar{1}$ 2⟩ type. (d) Key to the diffraction pattern in (c). Spots marked DD were due to double diffraction.

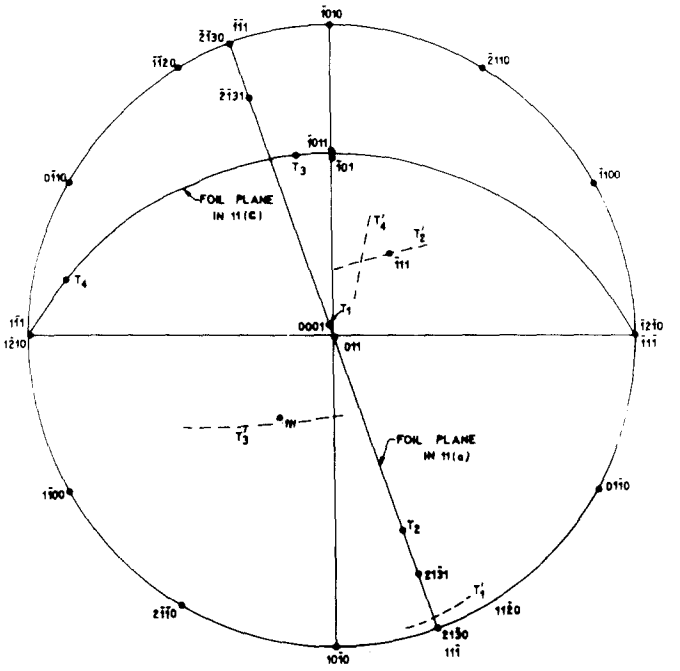

Figure 12 Stereogram illustrating the orientation relationship between the α-Zr(Cr) and $ZrCr_2$ phases. Foil planes corresponding to the diffraction patterns in Fig. 11a and c have been marked. It could be seen that the following orientation relationship is consistent with the two sets of superimposed reciprocal lattice sections represented by the great circles: $(0\,0\,0\,1)_\alpha \| (0\,1\,1)_{ZrCr_2}$, $[1\,\bar{2}\,1\,0]_\alpha \| [1\,\bar{1}\,1]_{ZrCr_2}$, $[2\,1\,\bar{3}\,0]_\alpha \| [1\,1\,\bar{1}]_{ZrCr_2}$. Habit plane traces ($T_1$, T_2 etc.) are indicated on the respective foil plane traces. Single surface trace analysis showed that the habit planes corresponded to $\{1\,1\,1\}_{ZrCr_2}$ type planes. T_1', T_2' etc. indicate the traces corresponding to the poles T_1, T_2 etc.

such a stereographic plot, from which it could be seen that $(1\,\bar{1}\,1)$ pole of $ZrCr_2$ should coincide with the $(1\,\bar{2}\,1\,0)_\alpha$ pole. This was indeed observed in the diffraction pattern shown in Fig. 11c. The foil plane trace corresponding to this pattern is also marked in Fig. 12. In view of these observations, the orientation relation between the α-Zr(Cr) and $ZrCr_2$ phases could be described as:

$$\{0\,0\,0\,1\}_\alpha \| \{0\,1\,1\}_{ZrCr_2}$$

and

$$\langle 1\,\bar{2}\,1\,0\rangle_\alpha \| \langle 1\,\bar{1}\,1\rangle_{ZrCr_2}.$$

This orientation relation was also confirmed on a different reciprocal lattice section as illustrated earlier in Fig. 6.

Single surface trace analysis showed that the majority of the straight line segments defining the precipitate boundaries were parallel to the $\{1\,1\,1\}$ traces of $ZrCr_2$. It could be seen, using the orientation relation, that different variants of the $\{1\,1\,1\}$ planes were parallel to some low index planes of the matrix such as $(2\,1\,\bar{3}\,0)$ and $(1\,\bar{2}\,1\,0)$. From the limited number of trace analyses carried out, it was not possible to establish unambiguously the plane that most frequently matched with the flat face of the precipitates. However, in view of the near equality of the interplanar spacings of the $\{2\,1\,\bar{3}\,0\}_\alpha$ and the $\{4\,4\,4\}_{ZrCr_2}$ planes (a difference of about 1.8%) and the close lattice matching along directions in these planes. (e.g. a difference of only about 1.2% along $\langle 0\,0\,0\,1\rangle \| \langle 0\,1\,\bar{1}\rangle$) it appeared reasonable to take the $\{2\,1\,\bar{3}\,0\}_\alpha$ planes as the habit planes in terms of the matrix.

5. Conclusions

On the basis of the observations described and discussed here, the following conclusions could be drawn:

(1) the precipitation of $ZrCr_2$ particles could not be suppressed even on rapidly quenching the alloy from the beta phase. Ageing at low temperatures gave rise to a bimodal precipitate size distribution. A significant amount of precipitate coarsening occurred on tempering the martensite at 700° C;

(2) the orientation relationship between the α-Zr(Cr) and the $ZrCr_2$ phases could be described as:

$$\{0\,0\,0\,1\}_\alpha \| \{0\,1\,1\}_{ZrCr_2}$$

and

$$\langle 1\,\bar{2}\,1\,0\rangle \| \langle 1\,\bar{1}\,1\rangle_{ZrCr_2}.$$

Acknowledgements

The authors are thankful to Dr V. M. Padmanabhan and Dr M. K. Asundi for their keen interest in this work and for helpful discussions. The experimental assistance of Miss J. Agarwal is gratefully acknowledged.

References

1. W. B. PEARSON, "A Handbook of Lattice Spacings and Structures of Metals and Alloys", Vol. 2 (Pergamon Press, Oxford, 1967) p. 67.
2. L. H. KEYS, G. JOHANSON and A. S. MALIN, *J. Nucl. Mater.* **59** (1976) 137.
3. W. ROSTOKER, *J. Metals* **5** (1953) 304.
4. R. P. ELLIOTT, Technical Report No. 1 OSR-TN-247, Illinois Institute of Technology (1954).
5. S. P. ALISOVA, P. B. BUDBERG and K. I. SHAKHOVA, *Sov. Phys. Cryst.* (English Translation) 9 (3) (1964) 343.
6. C. B. JORDAN and POL DUWEZ, Progress Report, 20–196, CIT Jet Propulsion Lab., 16 June (1953).
7. YUAN-SHOU SHEN and O. G. PAASCHE, *Trans. AIME* **242** (1968) 2241.
8. W. M. RUMBALL and F. G. ELDER, *J. Less Common Metals* **19** (1969) 345.
9. A. K. SINHA, *Prog. Mater. Sci.* **15** (2) (1972) 81.
10. E. TEATUM, K. GSCHNEIDNER and J. WABER, Los Alamos Scientific Lab. Report No. LA-2345 (1960).
11. R. I. JAFFEE, *Prog. Met. Phys.* 7 (1958) 65.
12. H. I. AARONSON, C. LAIRD and K. R. KINSMAN, "Phase Transformations" (American Society for Metals, Ohio, 1970) p. 313.

Received 9 August and accepted 2 October 1978.